nanomaterials

MDPI

Article

Computational Evaluation of Al-Decorated g-CN Nanostructures as High-Performance Hydrogen-Storage Media

Peng Gao [3,4,†], Xihao Chen [1,2,†], Jiwen Li [5], Yue Wang [6], Ya Liao [1], Shichang Liao [7], Guangyu Zhu [1], Yuebin Tan [8] and Fuqiang Zhai [1,*]

[1] School of Materials Science and Engineering, Chongqing University of Arts and Sciences, Chongqing 402160, China; xihaochen@cqwu.edu.cn (X.C.); liao__ya@163.com (Y.L.); zhuguangyu@cqwu.edu.cn (G.Z.)
[2] State Key Laboratory of Precision Spectroscopy, East China Normal University, Shanghai 200062, China
[3] School of Chemistry and Molecular Bioscience, University of Wollongong, Wollongong, NSW 2500, Australia; pg177@uowmail.edu.au
[4] Molecular Horizons, University of Wollongong, Wollongong, NSW 2500, Australia
[5] College of Physics and Electronic Engineering, Northwest Normal University, Lanzhou 730070, China; jiwenli369@163.com
[6] Department of Electrical Engineering, Hanyang University, Seoul 04763, Korea; wangyue9471@hanyang.ac.kr
[7] School of Materials and Energy, Southwest University, Chongqing 400715, China; lsc19980403@email.swu.edu.cn
[8] Department of Biochemistry and Molecular & Cellular Biology, Georgetown University, Washington, DC 20007, USA; ty157@georgetown.edu
* Correspondence: zhaifuqiang@cqwu.edu.cn.
† These authors contributed equally to this work.

check for updates

Citation: Gao, P.; Chen, X.; Li, J.; Wang, Y.; Liao, Y.; Liao, S.; Zhu, G.; Tan, Y.; Zhai, F. Computational Evaluation of Al-Decorated g-CN Nanostructures as High-Performance Hydrogen-Storage Media. *Nanomaterials* **2022**, *12*, 2580. https://doi.org/10.3390/nano12152580

Academic Editor: Carlos Miguel Costa

Received: 23 June 2022
Accepted: 26 July 2022
Published: 27 July 2022

Publisher's Note: MDPI stays neutral with regard to jurisdictional claims in published maps and institutional affiliations.

Abstract: Density functional theory (DFT) calculations were employed to solve the electronic structure of aluminum (Al)-doped g-CN and further to evaluate its performance in hydrogen storage. Within our configurations, each 2 × 2 supercell of this two-dimensional material can accommodate four Al atoms, and there exist chemical bonding and partial charge transfer between pyridinic nitrogen (N) and Al atoms. The doped Al atom loses electrons and tends to be electronically positive; moreover, a local electronic field can be formed around itself, inducing the adsorbed H_2 molecules to be polarized. The polarized H_2 molecules were found to be adsorbed by both the N and Al atoms, giving rise to the electrostatic attractions between the H_2 molecules and the Al-doped g-CN surface. We found that each 2 × 2 supercell can adsorb at most, 24 H_2 molecules, and the corresponding adsorption energies ranged from −0.11 to −0.31 eV. The highest hydrogen-storage capacity of the Al-doped g-CN can reach up to 6.15 wt%, surpassing the goal of 5.50 wt% proposed by the U.S. Department of Energy. Additionally, effective adsorption sites can be easily differentiated by the electronic potential distribution map of the optimized configurations. Such a composite material has been proven to possess a high potential for hydrogen storage, and we have good reasons to expect that in the future, more advanced materials can be developed based on this unit.

Keywords: DFT; ab initio; molecular dynamics

1. Introduction

Under the context of a global energy shortage and high emissions of greenhouse gases, finding high-performance sources of renewable energy has become increasingly crucial. Hydrogen had long been regarded as the 'fuel of future', due to its high calorific value of combustion and low environmental pollution [1]. For instance, the vehicles powered by hydrogen cells release zero emissions of CO_2 if the hydrogen fuel can be produced from renewable circulations [2,3]. However, in real practice, to fully utilize hydrogen as an ideal energy carrier is usually challenging, with the largest hurdle being associated with

its delivery and storage operations [4,5]. Traditional technologies for hydrogen storage usually require compression under high pressures (around 700 bar), possibly giving rise to safety issues; therefore, the development of materials-based storage media remains to be an important goal. During the past decades, various novel materials have been characterized and evaluated by researchers for hydrogen storage, including liquid hydrocarbons [6], metal hydrides [7–10], boron-containing compounds [11–16], etc. An ideally designed material for hydrogen storage should be competitive in both adsorption strength and operational conveniences, instead of underscoring just one attribute over the other.

Over the past decades, two-dimensional (2D) graphene-like materials with porous structures were found to possess several superior properties for energy storage [17–27]. In one aspect, these kinds of graphene-like materials tend to possess large surface areas for efficient adsorptions, and some kinds of material storage capacities can even surpass 10 wt% [17–30]; in another aspect, their natural porosity enables them to easily accommodate active atoms or clusters to favorably change their electronic structures, and to further enhance their adsorption abilities [31–40]. In recent years, the successful synthesis of one promising graphene-like 2D material, carbon nitride (g-CN), was realized through the reaction between Na and $C_3N_3Cl_3$, and under solvothermal conditions [41], the optimized configuration is presented in Figure 1. In each of its units, there exist six pyridinic N atoms, and the band gap is estimated to be 2.73 eV. With such a porosity, the g-CN can easily accommodate metal atoms for functional modification. Chen et al. reported that with the decoration of Li atoms, g-CN displays high performance in hydrogen storage [42]. It had been well recognized that the doped metal atoms can bind with pristine 2D materials, and that the binding structure can furthermore impact on its adsorption capabilities [35]; however, to fundamentally identify the correlation between the electronic structure of the metal-doped g-CN and its performance in gas adsorption, more studies are needed.

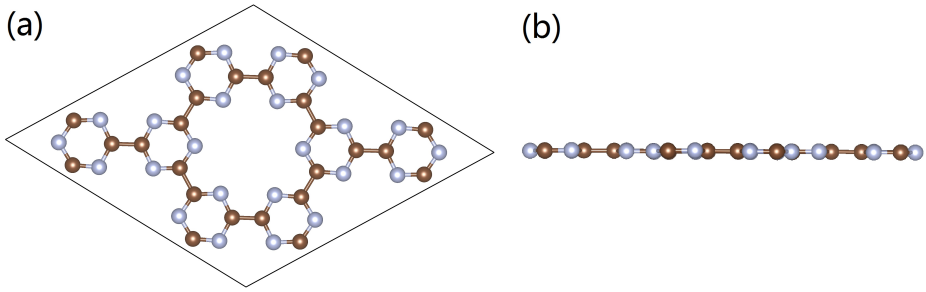

Figure 1. (**a**,**b**) Optimized configuration of the g-CN monolayer. Brown and silver spheres represent C and N atoms, respectively.

Metallic Al has three outer electrons, making it easy for Al to bind with atoms with a high electro-withdrawing power. Thus, in this study, we computationally solved the electronic structure of Al-doped g-CN by employing density functional theory (DFT) calculations. Furthermore, we also evaluated its potential in hydrogen storage and identified the factors that are crucial for its performance. We believe that the findings provided by this study will be valuable and will largely assist in the development of novel 2D materials with improved performance for renewable energy storage.

2. Materials and Methods

DFT calculations were conducted with the Vienna Ab-initio Simulation Package (VASP) [43,44]. The lattice parameters of the g-CN supercell were set to $a = b = 14.24$ Å. The generalized gradient approximation developed by Perdew–Burke–Ernzerhof [45,46] was applied for exchange-correlation energies calculations. A plane wave basis was employed to expand the electronic states, and the energy cutoff was set to 520 eV. The projector augmented wave method was applied to describe the core–valence interactions [47]. The Al-doped g-CN system contains 52 atoms; therefore, for a 2 × 2 supercell, gamma-centered

k-point grid of 3 × 3 × 1 was applied for Brillouin zone sampling [48,49]. Van der Waals corrections were considered by implementing the DFT-D2 method [44]. A 30 Å vacuum layer was adopted to isolate the periodic slabs along the *c* direction. Structural relaxations were realized using the conjugate-gradient algorithm. The charge transfer among the doped Al atoms and the pristine g-CN surface were estimated using the Bader charge analysis [50]. The applied convergence criterion of the Hellmann–Feynman forces was set to 0.01 eV/Å, and 10^{-5} eV for the electronic structures calculations and geometry optimizations. All the computational parameters were set with a balance between cost and accuracy.

For the Al atoms on the pristine g-CN, the adsorption energy was obtained by the equation below:

$$E_{ad}(\mathrm{Al}) = [E(\mathrm{Al}_k \circ \mathrm{C_{24}N_{24}}) - E(\mathrm{C_{24}N_{24}}) - kE(\mathrm{Al})]/k(\mathrm{Al}), \quad (1)$$

where k(Al) is the number of Al atoms, and E indicates an energy term. The adsorption energy per H_2 molecule was calculated with the following equation:

$$E_{ad}(\mathrm{H_2}) = [E(n\mathrm{H_2} \bullet \mathrm{Al} \circ \mathrm{C_{24}N_{24}}) - E(\mathrm{Al} \circ \mathrm{C_{24}N_{24}}) - nE(\mathrm{H_2})]/n(\mathrm{H_2}), \quad (2)$$

where $n(H_2)$ is the number of H_2 molecules that are adsorbed by the Al-doped g-CN surface.

3. Results and Discussion

3.1. Structural Features of Al-Doped g-CN

To identify the possible adsorption sites for Al atoms on the surface of g-CN, sites close to the pyridinic N atoms either parallel or slightly above the plane were considered. After DFT optimizations, we found that the favorable adsorption site is located in the vicinity of two neighboring N atoms where the adsorbed Al atom is slightly off the plane. The corresponding adsorption energy per Al atom is −4.76 eV; and it tends to bind with the pyridinic N atoms. The specific configurations are presented in Figure 2. It is highly possible that such a binding between Al and N atoms is associated with charge transfer (more details will be discussed in the following section). In this study, we merely focused on the configuration that has one single Al atom at each pore of g-CN; the reason for this lies in the fact that due to steric hindrance, the accommodation of multiple metal atoms with larger sizes in the same pore may eliminate the adsorption capacity of the H_2 molecules. However, for the doped atoms or clusters with a smaller size, such as Li, NLi_4, etc., the placement of multiple units in one pore may enhance the adsorption performance.

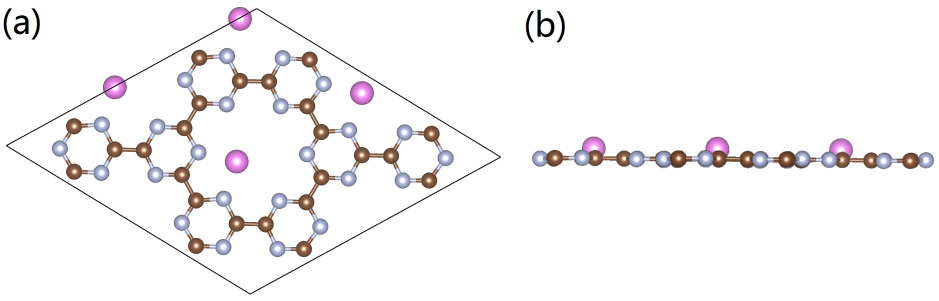

Figure 2. (**a**,**b**) Optimized configuration of the Al-doped g-CN monolayer. Brown, silver, and pink spheres represent C, N, and Al atoms, respectively.

From the calculated density of states (DOSs), we found the conductivity of Al-doped g-CN was enhanced, further confirming our presumption that there exist binding and charge transfers between the pyridinic N and adsorbed Al atoms. The partial density of states (PDOS) of pristine g-CN are presented for the 2p and 2s orbitals of C/N atoms in Figure 3a, and it is notable that these two orbitals are hybridized with each other. With the addition of Al atoms, we noticed that the mid-band states appear at the Fermi level, as can be seen in Figure 3b, and the overlap between the 3s/3p orbitals from the Al atoms

and the hybrid orbitals of the C/N atoms further indicate the chemical binding and charge transfer between the Al atoms and g-CN. It is highly possible that the 3s/3p electrons of Al atoms are first hybridized, and then the Al atoms can bind with the two neighboring N atoms. Additionally, due to the fact that C and N are hybridized, the electrons from Al atoms can be transferred to the whole surface of g-CN; therefore, the electronic structure of g-CN may be largely changed. To clearly elucidate the chemical interactions between the Al atoms and g-CN, a Bader analysis was performed; the estimated amount of transferred charge from Al atoms is 1.2 e^-. Such a value is smaller than that of Mg atoms [29], and we can further realize that the overall electronic structure of the metal-doped 2D materials is also associated with the electron-donating power of the deposited metal atoms. The charge density difference for Al-doped g-CN is presented in Figure 4, and we can see that the higher electronegativity of C/N makes them easily obtain electrons from the Al atoms. This is consistent with our discussion. Moreover, we also notice that the doped Al atom loses electrons and tends to be polarized, and a local electronic field with some regions displaying a higher electropositivity can be formed around it. In fact, the addition of Al atoms can successfully transform the semiconducting g-CN into a conducting one. We can also expect the Al-doped g-CN with a superior electronic structure can perfom well in H_2 adsorptions.

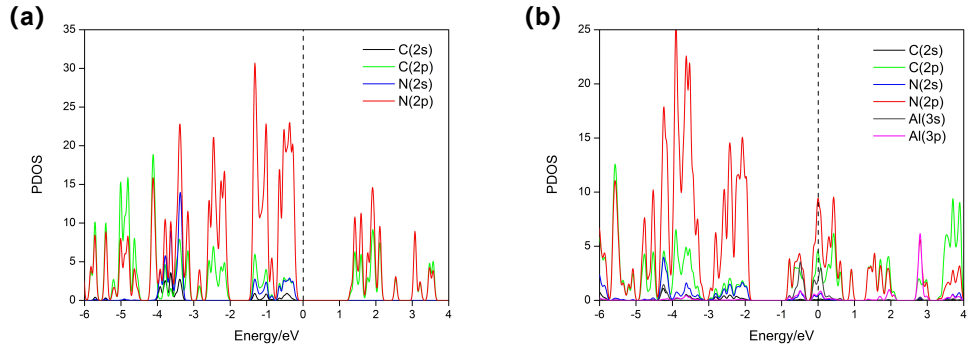

Figure 3. (**a**,**b**) The PDOS of the pristine g-CN and Al-doped g-CN for selected N, C, and Al atoms. The energy was plotted with respect to the Fermi energy.

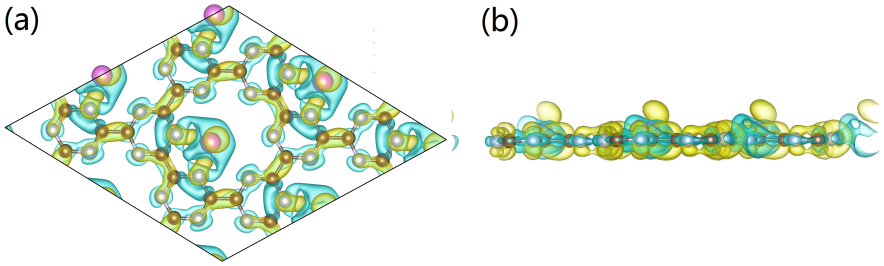

Figure 4. (**a**,**b**) Charge density difference for the Al-doped g-CN. Yellow regions indicate charge gain and the blue regions indicate charge loss. The isosurface of charge density is 0.0026 e/Bohr^3.

The thermodynamics stability of Al-doped g-CN was also evaluated in this study. First-principles molecular dynamics (MD) simulations of this composite material were performed under NVT ensemble; as can be seen from Figure 5, at a temperature of 300 K, its structure is proven to be stable, further demonstrating its applicability in real practice.

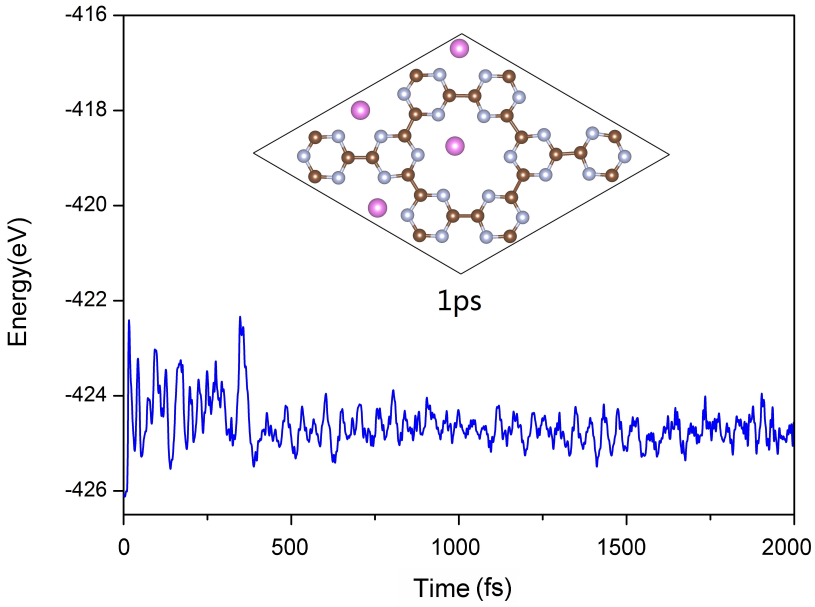

Figure 5. First−principles MD simulation of the Al-doped g-CN at a temperature of 300 K. The time step is set to 0.5 fs.

3.2. Hydrogen-Storage Performance Using Al-Doped g-CN

After clarifying the structural features of the Al-doped g-CN, we continue to evaluate its performance in hydrogen storage. The optimized configurations of Al-doped g-CN with multiple adsorbed H_2 molecules are presented in Figure 6. To detect suitable adsorption sites, we referred to the map of electronic potential distribution, as shown in Figure 7. It is observable that there are many active sites of adsorption, around the Al/N atoms. Thus, we placed H_2 molecules around these Al/N atoms, and ab initio-based calculations were performed to locate the minimum of potential energy surface. As discussed in the previous section, each Al atom had transferred its partial charges to the surface of g-CN, and displayed an electropositive charge. Then, the local electronic field around the Al atoms can further induce the polarization of nearby H_2 molecules, enhancing its adsorption ability. From the map of charge density difference for Al-doped g-CN with adsorbed H_2, as presented in Figure 6, we noticed that within each polarized H_2 molecule, one H loses electrons and shows electronegativity, while the other gains electrons and displays electropositivity; such a phenomenon is also observable for other metal-decorated 2D materials. Thus, we can conclude that the electrostatic interaction among Al atoms and these polarized H_2 molecules can be attributed to a dipole-charged one. The highest adsorption energy of a single H_2 molecule by an Al atom can reach up to −0.309 eV.

To further estimate the highest adsorption capacity of H_2, many possible sites were considered, and we found that each 2 × 2 supercell containing four Al atoms can accommodate, at most, 36 H_2 molecules. Besides the region surrounding the Al atoms, H_2 molecules can also be adsorbed by C/N atoms. For these adsorbed H_2 molecules in the vicinity of non-metallic sites, they tend to be parallel with the plane. Such a binding geometry may be largely caused by polarization effects, as the middle region of H−H bonds tend to show electropositivity, and this region can interact with the C/N atoms that are highly electronegative to form a hydrogen bonding-like interaction (more details can be found in Figures 7 and 8). The H_2 molecules distributed around the Al atoms tend to be bound vertically to the plane, similar to the case of Mg doping. The adsorption energies of H_2, the lengths of the H−H bonds, and the adsorption capacities of each configuration are presented in Table 1; it is observable that all H−H bonds in optimized configurations are slightly stretched. It is notable that the averaged adsorption energy per H_2 decreases with the total adsorption capacity, indicating that for each active site, due to steric hindrance, there exists a maximum number of adsorbed H_2 molecules.

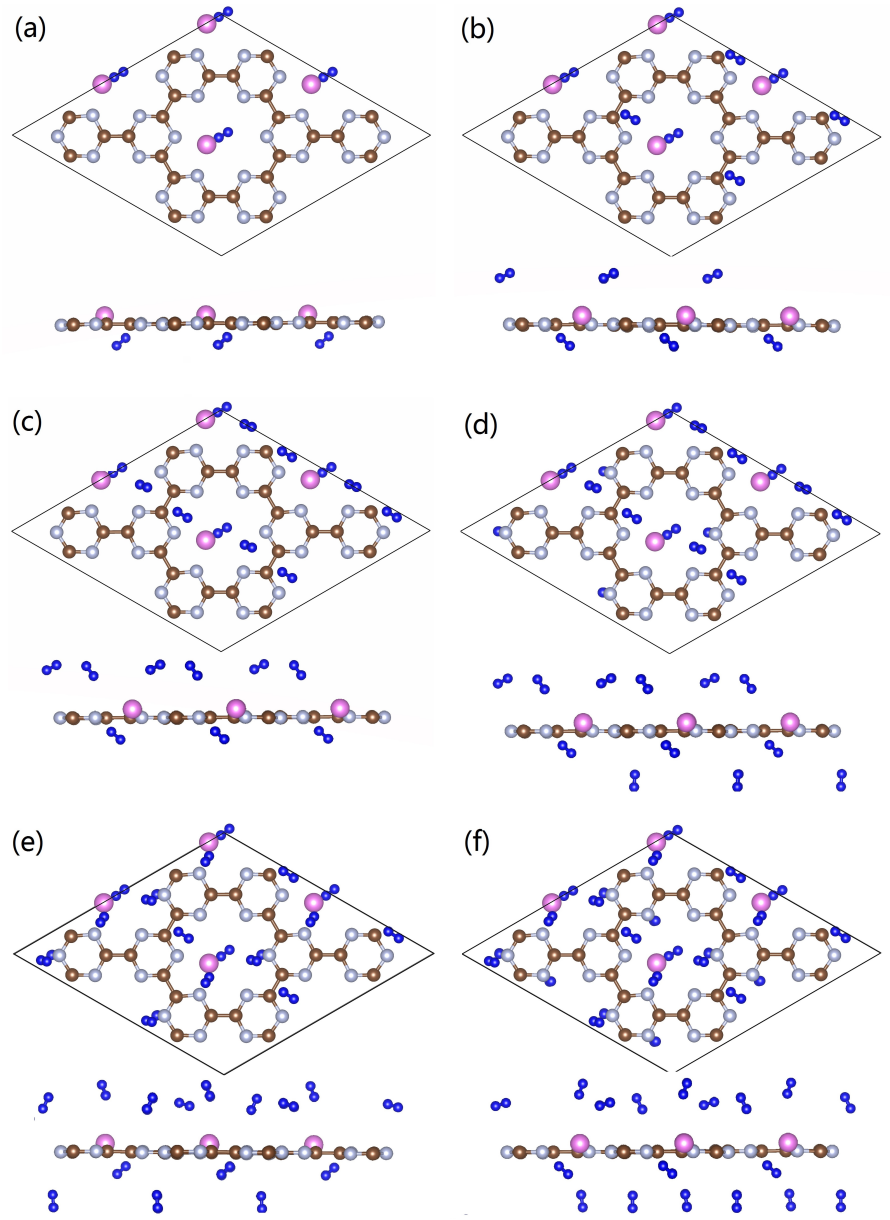

Figure 6. (**a**–**f**) The optimized configurations of the Al-doped g-CN with multiple adsorbed H_2 molecules (4–24).

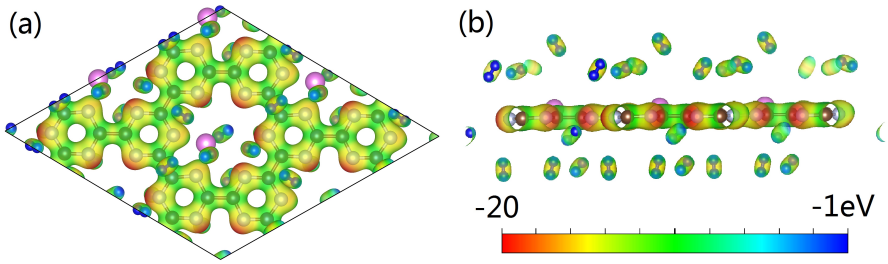

Figure 7. (**a**,**b**) The map of electrostatic potential distribution for the Al-doped g-CN with adsorbed H_2 molecules.

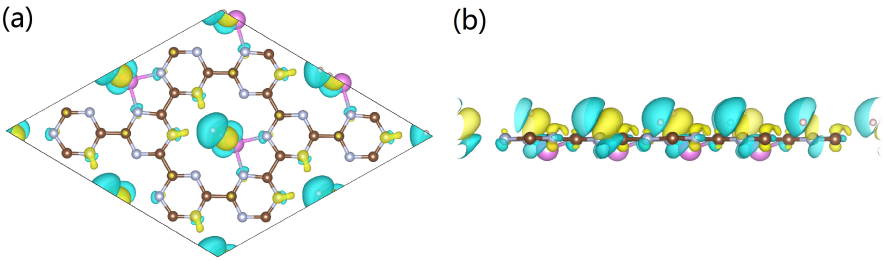

Figure 8. (**a**,**b**) Charge density difference for the Al-doped g-CN with multiple adsorbed H_2 molecules. Yellow regions indicate charge gain and blue regions indicate charge loss. The isosurface of charge density is set to 0.0016 e/Bohr^3.

Table 1. The adsorption energy (E_{Ad}, in eV) per H_2 on Al-doped g-CN, the averaged H−H bonding length (in Å), and the hydrogen-storage capacity (wt%).

System	Adsorption E	H−H Bond	Capacity
$Al_4C_{24}N_{24} + 4H_2$	−0.31	0.787	1.10
$Al_4C_{24}N_{24} + 8H_2$	−0.19	0.770	2.14
$Al_4C_{24}N_{24} + 12H_2$	−0.15	0.765	3.17
$Al_4C_{24}N_{24} + 16H_2$	−0.13	0.762	4.12
$Al_4C_{24}N_{24} + 20H_2$	−0.13	0.762	5.18
$Al_4C_{24}N_{24} + 24H_2$	−0.11	0.759	6.15

4. Conclusions

The electronic structure of Al-doped g-CN was systematically solved via ab initio calculations, and its potential for hydrogen storage was evaluated. With the addition of Al atoms, the highest hydrogen-storage capacity of g-CN can reach up to 6.15 wt%. The Al atoms can bind with N atoms, and there exists a partial charge transfer between these Al atoms and the pristine g-CN. The adsorption energy of each Al atom in the pore of g-CN is around −4.67 eV. The higher electropositivity of the Al atoms can induce the polarization of the adsorbed H_2 molecules, further enhancing the electrostatic interactions among them. The electronic potential distribution map of Al-doped g-CN was also presented in this study, and the most active sites for adsorption, along with the corresponding adsorption energies, were described. With this fundamental investigation, the adsorption mechanism of graphene-like 2D materials was clearly elucidated; and the most important factors associated with their adsorption performance were summarized. We believe that the findings provided by this study will largely facilitate the development of advanced nanostructure-based materials.

Author Contributions: P.G., X.C. and F.Z. outlined the whole project and designed the calculations. P.G., X.C. and J.L. carried out the calculations. P.G., X.C., J.L., Y.T., Y.W., Y.L., S.L. and G.Z. worked on data analysis. P.G. and X.C. contributed to the writing of this article. All authors have read and agreed to the published version of the manuscript.

Funding: This research was funded by the Talent Introduction Research Funds of CQWU grant number R2019FXCo7 and the Public Service Platform for the Industrialization of Technological Innovation Achievements in the Field of Robot and Intelligent Manufacturing of Chongqing grant number 2019-00900-1-1.

Data Availability Statement: The data that support the findings of this study are available from the corresponding author, upon reasonable request.

Acknowledgments: We thank the Australian Government for providing P.G. an Australian International Postgraduate Award scholarship to support his Ph.D study, during which (from 2017 to 2020) P.G. outlined and completed this project. We also wish to acknowledge the NCI National Facility systems at the Australian National University, with the National Computational Merit Allocation

Scheme, supported by the Australian Government (Project id: v15). The work by X.C. and F.Z. was supported by the Talent Introduction Research Funds of CQWU (Grant No. R2019FXCo7) and the Public Service Platform for the Industrialization of Technological Innovation Achievements in the Field of Robot and Intelligent Manufacturing in Chongqing (Grant No. 2019-00900-1-1).

Conflicts of Interest: The authors declare no conflicts of interest.

References

1. Züttel, A. Hydrogen storage methods. *Naturwissenschaften* **2004**, *91*, 157–172. [CrossRef]
2. Allendorf, M.D.; Hulvey, Z.; Gennett, T.; Ahmed, A.; Autrey, T.; Camp, J.; Seon Cho, E.; Furukawa, H.; Haranczyk, M.; Head-Gordon, M.; et al. An assessment of strategies for the development of solid-state adsorbents for vehicular hydrogen storage. *Energy Environ. Sci.* **2018**, *11*, 2784–2812. [CrossRef]
3. U.S. Department of Energy. *Hydrogen and Fuel Cell Technologies Office Multi-Year Research, Development and Demonstration Plan;* U.S. Department of Energy: Washington, DC, USA, 2014.
4. Züttel, A. Materials for hydrogen storage. *Mater. Today* **2003**, *6*, 24–33. [CrossRef]
5. Huang, Z.; Autrey, T. Boron–nitrogen–hydrogen (BNH) compounds: Recent developments in hydrogen storage, applications in hydrogenation and catalysis, and new syntheses. *Energy Environ. Sci.* **2012**, *5*, 9257–9268. [CrossRef]
6. Teichmann, D.; Stark, K.; Müller, K.; Zöttl, G.; Wasserscheid, P.; Arlt, W. Energy storage in residential and commercial buildings via Liquid Organic Hydrogen Carriers (LOHC). *Energy Environ. Sci.* **2012**, *5*, 9044–9054. [CrossRef]
7. Graetz, J. New approaches to hydrogen storage. *Chem. Soc. Rev.* **2009**, *38*, 73–82. [CrossRef] [PubMed]
8. Bogdanović, B.; Schwickardi, M. Ti-doped alkali metal aluminium hydrides as potential novel reversible hydrogen storage materials1: Invited paper presented at the International Symposium on Metal−Hydrogen Systems. *J. Alloys Compd.* **1997**, *253–254*, 1–9.
9. Sakintuna, B.; Lamari-Darkrim, F.; Hirscher, M. Metal hydride materials for solid hydrogen storage: A review. *Int. J. Hydrog. Energy* **2007**, *32*, 1121–1140. [CrossRef]
10. Züttel, A.; Wenger, P.; Rentsch, S.; Sudan, P.; Mauron, P.; Emmenegger, C. $LiBH_4$ a new hydrogen storage material. *J. Power Sources* **2003**, *118*, 1–7. [CrossRef]
11. Gao, P.; Huang, Z.; Yu, H. Exploration of the Dehydrogenation Pathways of Ammonia Diborane and Diammoniate of Diborane by Molecular Dynamics Simulations Using Reactive Force Fields. *J. Phys. Chem. A* **2020**, *124*, 1698–1704. [CrossRef] [PubMed]
12. Luo, W.; Zakharov, L.N.; Liu, S.Y. 1,2-BN Cyclohexane: Synthesis, Structure, Dynamics, and Reactivity. *J. Am. Chem. Soc.* **2011**, *133*, 13006–13009. [CrossRef] [PubMed]
13. Luo, W.; Campbell, P.G.; Zakharov, L.N.; Liu, S.Y. A Single-Component Liquid-Phase Hydrogen Storage Material. *J. Am. Chem. Soc.* **2011**, *133*, 19326–19329. [CrossRef] [PubMed]
14. Campbell, P.G.; Zakharov, L.N.; Grant, D.J.; Dixon, D.A.; Liu, S.Y. Hydrogen Storage by Boron-Nitrogen Heterocycles: A Simple Route for Spent Fuel Regeneration. *J. Am. Chem. Soc.* **2010**, *132*, 3289–3291. [CrossRef] [PubMed]
15. Gao, P.; Zhang, J. Understanding the Dehydrogenation Pathways of Ammonium Octahydrotriborate ($NH_4B_3H_8$) by Molecular Dynamics Simulations with the Reactive Force Field (ReaxFF). *Adv. Theory Simul.* **2020**, *3*, 2000139. [CrossRef]
16. Gao, P.; Zhang, J. Understanding the Intra-Molecular Proton Transfer of Octahydrotriborate and Exploring the Dehydrogenation Pathways of $NH_4B_3H_8$ by DFT Calculations. *Adv. Theory Simul.* **2021**, *4*, 2000287. [CrossRef]
17. Holst, J.R.; Gillan, E.G. From Triazines to Heptazines: Deciphering the Local Structure of Amorphous Nitrogen-Rich Carbon Nitride Materials. *J. Am. Chem. Soc.* **2008**, *130*, 7373–7379. [CrossRef]
18. Thomas, A.; Fischer, A.; Goettmann, F.; Antonietti, M.; Müller, J.O.; Schlögl, R.; Carlsson, J.M. Graphitic carbon nitride materials: variation of structure and morphology and their use as metal-free catalysts. *J. Mater. Chem.* **2008**, *18*, 4893–4908. [CrossRef]
19. Dong, G.; Zhang, Y.; Pan, Q.; Qiu, J. A fantastic graphitic carbon nitride (g-C_3N_4) material: Electronic structure, photocatalytic and photoelectronic properties. *J. Photochem. Photobiol .C Photochem. Rev.* **2014**, *20*, 33–50. [CrossRef]
20. Wei, W.; Jacob, T. Strong excitonic effects in the optical properties of graphitic carbon nitride g-C_3N_4 from first principles. *Phys. Rev. B* **2013**, *87*, 085202. [CrossRef]
21. Liu, G.; Xue, M.; Liu, Q.; Yang, H.; Zhou, Y. Facile synthesis of C-doped hollow spherical g-C_3N_4 from supramolecular self-assembly for enhanced photoredox water splitting. *Int. J. Hydrog. Energy* **2019**, *44*, 25671–25679. [CrossRef]
22. Algara-Siller, G.; Severin, N.; Chong, S.Y.; Björkman, T.; Palgrave, R.G.; Laybourn, A.; Antonietti, M.; Khimyak, Y.Z.; Krasheninnikov, A.V.; Rabe, J.P.; et al. Triazine-Based Graphitic Carbon Nitride: A Two-Dimensional Semiconductor. *Angew. Chem. Int. Ed. Engl.* **2014**, *53*, 7450–7455. [CrossRef]
23. Jürgens, B.; Irran, E.; Senker, J.; Kroll, P.; Müller, H.; Schnick, W. Melem (2,5,8-Triamino-tri-s-triazine), an Important Intermediate during Condensation of Melamine Rings to Graphitic Carbon Nitride: Synthesis, Structure Determination by X-ray Powder Diffractometry, Solid-State NMR, and Theoretical Studies. *J. Am. Chem. Soc.* **2003**, *125*, 10288–10300. [CrossRef]
24. Wang, G.; Zhou, F.; Yuan, B.; Xiao, S.; Kuang, A.; Zhong, M.; Dang, S.; Long, X.; Zhang, W. Strain-Tunable Visible-Light-Responsive Photocatalytic Properties of Two-Dimensional CdS/g-C_3N_4: A Hybrid Density Functional Study. *Nanomaterials* **2019**, *9*, 244. [CrossRef]

25. Fina, F.; Callear, S.K.; Carins, G.M.; Irvine, J.T.S. Structural Investigation of Graphitic Carbon Nitride via XRD and Neutron Diffraction. *Chem. Mater.* **2015**, *27*, 2612–2618. [CrossRef]
26. Hussain, T.; Hankel, M.; Searles, D.J. Computational Evaluation of Lithium-Functionalized Carbon Nitride (g-C_6N_8) Monolayer as an Efficient Hydrogen Storage Material. *J. Phys. Chem. C* **2016**, *120*, 25180–25188. [CrossRef]
27. Gao, P.; Li, J.; Wang, G. Computational evaluation of superalkali-decorated graphene nanoribbon as advanced hydrogen storage materials. *Int. J. Hydrog. Energy* **2021**, *46*, 24510–24516. [CrossRef]
28. Liu, A.Y.; Cohen, M.L. Prediction of New Low Compressibility Solids. *Science* **1989**, *245*, 841–842. [CrossRef]
29. Gao, P.; Li, J.; Zhang, J.; Wang, G. Computational exploration of magnesium-decorated carbon nitride (g-C_3N_4) monolayer as advanced energy storage materials. *Int. J. Hydrog. Energy* **2021**, *46*, 21739–21747. [CrossRef]
30. Chen, X.; Li, J.W.; Dou, X.; Gao, P. Computational evaluation of Mg-decorated g-CN as clean energy gas storage media. *Int. J. Hydrog. Energy* **2021**, *46*, 35130–35136 . [CrossRef]
31. Nair, A.A.; Sundara, R.; Anitha, N. Hydrogen storage performance of palladium nanoparticles decorated graphitic carbon nitride. *Int. J. Hydrog. Energy* **2015**, *40*, 3259–3267. [CrossRef]
32. Ruan, L.; Xu, G.; Gu, L.; Li, C.; Zhu, Y.; Lu, Y. The physical properties of Li-doped g-C_3N_4 monolayer sheet investigated by the first-principles. *Mater. Res. Bull.* **2015**, *66*, 156–162. [CrossRef]
33. Zhu, G.; Lü, K.; Sun, Q.; Kawazoe, Y.; Jena, P. Lithium-doped triazine-based graphitic C_3N_4 sheet for hydrogen storage at ambient temperature. *Comput. Mater. Sci.* **2014**, *81*, 275–279. [CrossRef]
34. Zhang, Y.; Sun, H.; Chen, C. New template for metal decoration and hydrogen adsorption on graphene-like C_3N_4. *Phys. Lett. A* **2009**, *373*, 2778–2781. [CrossRef]
35. Wu, M.; Wang, Q.; Sun, Q.; Jena, P. Functionalized Graphitic Carbon Nitride for Efficient Energy Storage. *J. Phys. Chem. C* **2013**, *117*, 6055–6059. [CrossRef]
36. Gao, Z.; Wang, L.; Wang, L.; Huang, J.; She, H.; Wang, Q. Construction of heterostructured g-C_3N_4@TiATA/Pt composites for efficacious photocatalytic hydrogen evolution. *Int. J. Hydrog. Energy* **2019**, *44*, 24407–24417. [CrossRef]
37. Panigrahi, P.; Kumar, A.; Karton, A.; Ahuja, R.; Hussain, T. Remarkable improvement in hydrogen storage capacities of two-dimensional carbon nitride (g-C_3N_4) nanosheets under selected transition metal doping. *Int. J. Hydrog. Energy* **2020**, *45*, 3035–3045. [CrossRef]
38. Wei, J.; Huang, C.; Wu, H.; Kan, E. High-capacity hydrogen storage in Li-adsorbed g-C_3N_4. *Mater. Chem. Phys.* **2016**, *180*, 440–444. [CrossRef]
39. Tranca, D.C.; Seifert, G. A First-Principles Study of Metal-Decorated Graphene Nanoribbons for Hydrogen Storage. *Z. Phys. Chem.* **2016**, *230*, 791–808. [CrossRef]
40. Ngqalakwezi, A.; Nkazi, D.; Seifert, G.; Ntho, T. Effects of reduction of graphene oxide on the hydrogen storage capacities of metal graphene nanocomposite. *Catalysis Today* **2020**, *358*, 338–344. [CrossRef]
41. Li, J.; Cao, C.; Hao, J.; Qiu, H.; Xu, Y.; Zhu, H. Self-assembled one-dimensional carbon nitride architectures. *Diam. Relat. Mater.* **2006**, *15*, 1593–1600. [CrossRef]
42. Chen, Y.D.; Yu, S.; Zhao, W.H.; Li, S.F.; Duan, X.M. A potential material for hydrogen storage: A Li decorated graphitic-CN monolayer. *Phys. Chem. Chem. Phys.* **2018**, *20*, 13473–13477. [CrossRef]
43. Kresse, G.; Furthmüller, J. Efficient iterative schemes for ab initio total-energy calculations using a plane-wave basis set. *Phys. Rev. B* **1996**, *54*, 11169–11186. [CrossRef]
44. Grimme, S. Semiempirical GGA-type density functional constructed with a long-range dispersion correction. *J. Comput. Chem.* **2006**, *27*, 1787–1799. [CrossRef]
45. Perdew, J.P.; Wang, Y. Pair-distribution function and its coupling-constant average for the spin-polarized electron gas. *Phys. Rev. B* **1992**, *46*, 12947–12954. [CrossRef]
46. Perdew, J.P.; Burke, K.; Ernzerhof, M. Generalized Gradient Approximation Made Simple. *Phys. Rev. Lett.* **1996**, *77*, 3865–3868. [CrossRef]
47. Blöchl, P.E. Projector augmented-wave method. *Phys. Rev. B* **1994**, *50*, 17953–17979. [CrossRef]
48. Monkhorst, H.J.; Pack, J.D. Special points for Brillouin-zone integrations. *Phys. Rev. B* **1976**, *13*, 5188–5192. [CrossRef]
49. Chadi, D.J. Special points for Brillouin-zone integrations. *Phys. Rev. B* **1977**, *16*, 1746–1747. [CrossRef]
50. Bader, R. *Atoms in Molecules—A Quantum Theory*; Oxford University Press: Oxford, UK, 1990.